Dynamic Interfacial Reaction Rates from Electrochemistry-Mass Spectrometry

Krempl, Kevin; Hochfilzer, Degenhart; Scott, Soren B.; Kibsgaard, Jakob; Vesborg, Peter C.K.; Hansen, Ole; Chorkendorff, Ib

Published in:
Analytical Chemistry

Link to article, DOI:
10.1021/acs.analchem.1c00110

Publication date:
2021

Document Version
Peer reviewed version

Dynamic Interfacial Reaction Rates from Electrochemistry - Mass Spectrometry
-
Supporting Information

Kevin Krempl,[†] Degenhart Hochfilzer,[†] Soren B. Scott,[‡] Jakob Kibsgaard,[†] Peter C. K. Vesborg,[†] Ole Hansen,[¶] and Ib Chorkendorff[*,†]

† *Department of Physics, Technical University of Denmark, DK-2800 Kgs. Lyngby, Denmark*
‡ *Department of Materials, Imperial College London, SW7 2AZ, UK*
¶ *DTU Nanolab, Technical University of Denmark, DK-2800 Kgs. Lyngby, Denmark*

E-mail: ibchork@fysik.dtu.dk

Contents

Cyclic voltammetry

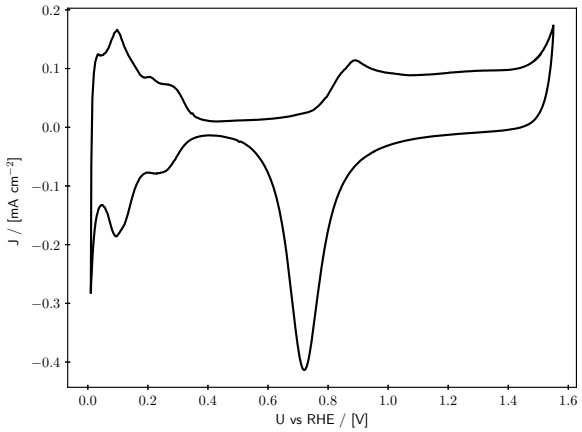

Figure S1: Steady-state cylcic voltammogram of the Pt electrode in 0.1 M $HClO_4$.

Mass transport model

The mass transport from the electrode surface to the gas-liquid interface inside the stagnant thin-layer electrochemical cell is described by Fick's law of diffusion. Because of the high aspect ratio of the modeled electrolyte volume ($\frac{d_{electrode}}{L} = \frac{5\,\mathrm{mm}}{0.1\,\mathrm{mm}} = 50$) and the assumption of an homogeneous current density distribution on the electrode, radial mass transport is neglected resulting in the following equation

$$\frac{\partial c_{l,i}}{\partial t} = D_i \frac{\partial^2 c_{l,i}}{\partial x^2}. \tag{1}$$

At the electrode surface at $x = L$, a time dependant flux boundary condition equivalent to the partial current density of the analyte is applied. Together with the liquid-gas interface at $x = 0$ being described by Henry's law, the boundary conditions in Eq. 2 and 3 are obtained

$$D_i \frac{\partial c_{l,i}}{\partial x}\Big|_{x=L} = \dot{n}_i(t) = \frac{J_i(t)}{n_e F} \tag{2}$$

$$c_{l,i}(x = 0) = \frac{1}{k_{H,i}} c_{g,i}. \tag{3}$$

Here $k_{H.i}$ is the dimensionless Henry volatility, n_e is the number of electons transfered per analyte molecule and F is Faraday's constant. The gas volume is assumed to be ideally mixed due to the fast diffusion of the analyte in the auxiliary gas (either He or Ar). A molar balance around the gas volume then yields the following equation

$$V_g \frac{dc_{g,i}}{dt} = A D_i \frac{\partial c_{l,i}}{\partial x}\Big|_{x=0} - c_{g,i}\dot{V}_{cap}. \tag{4}$$

Here A is the geometric surface area of the electrode and the capillary volume flow $\dot{V}_{cap}$ is calculated according to Trimarco[1] based on the properties of the auxiliary gas.

Next, the set of partial differential equations is non-dimensionalized with the following parameters

$$\hat{x} = \frac{x}{L} \tag{5}$$

$$\hat{t} = \frac{tD_i}{L^2} \tag{6}$$

$$\hat{c} = \frac{cL}{\int_0^\infty \dot{n}_i(\hat{t})d\hat{t}}. \tag{7}$$

The non-dimensionalized problem is then

$$\frac{\partial \hat{c}_{l,i}}{\partial \hat{t}} = \frac{\partial^2 \hat{c}_{l,i}}{\partial \hat{x}^2} \tag{8}$$

$$\frac{\partial \hat{c}_{l,i}}{\partial \hat{x}}\Big|_{\hat{x}=1} = \frac{\dot{n}_i(\hat{t})}{\int_0^\infty \dot{n}_i(\hat{t})d\hat{t}} \frac{L^2}{D_i} = \hat{n_i}(\hat{t}) \tag{9}$$

$$\hat{c}_{l,i}(\hat{x}=0) = \frac{1}{k_H}\hat{c}_{g,i} \tag{10}$$

$$\frac{d\hat{c}_{g,i}}{d\hat{t}} = \frac{AL}{V_g}\frac{\partial \hat{c}_{l,i}}{\partial \hat{x}}\Big|_{\hat{x}=0} - \hat{c}_{g,i}\frac{L^2\dot{V}_{cap}}{D_i V_g}. \tag{11}$$

By introducing the dimensionless residence time $\lambda = \frac{L^2\dot{V}_{cap}}{D_i V_g}$ and the geometric parameter $\kappa = \frac{AL}{V_g}$, Eq. 11 simplifies to the following

$$\frac{d\hat{c}_{g,i}}{d\hat{t}} = \kappa\frac{\partial \hat{c}_{l,i}}{\partial \hat{x}}\Big|_{\hat{x}=0} - \hat{c}_{g,i}\lambda. \tag{12}$$

The non-dimensionalized problem is then transformed into non-dimensionalized Laplace space according to Eq. 13

$$F(\hat{s}) = \mathcal{L}\{f(\hat{t})\} = \int_0^\infty f(\hat{t})e^{-\hat{s}\hat{t}}d\hat{t}. \tag{13}$$

This yields the following set of equations without partial derivatives anymore

$$\hat{s}\hat{C}_{l,i} = \frac{d^2\hat{C}_{l,i}}{d\hat{x}^2} \tag{14}$$

$$\frac{d\hat{C}_{l,i}}{d\hat{x}}\Big|_{\hat{x}=1} = \hat{N}_i(\hat{s}) \tag{15}$$

$$\hat{C}_{l,i}(\hat{x}=0) = \frac{1}{k_H}\hat{C}_{g,i} \tag{16}$$

$$\hat{s}\hat{C}_{g,i} = \kappa\frac{d\hat{C}_{l,i}}{d\hat{x}}\Big|_{\hat{x}=0} - \hat{C}_{g,i}\lambda. \tag{17}$$

Since the time derivative is eliminated in Laplace space the molar balance in Eq. 17 can be plugged into the boundary condition in Eq. 16 and a combined boundary condition is obtained according to Eq. 18

$$\frac{d\hat{C}_{l,i}}{d\hat{x}}\Big|_{\hat{x}=0} = k_H\frac{\hat{s}+\lambda}{\kappa}\hat{C}_{l,i}(\hat{x}=0). \tag{18}$$

The problem has now been simplified into an ordinary second order differential equation (Eq. 14) with a Neumann (Eq. 15) and a Robin (Eq. 18) boundary condition and can be solved analytically

yielding the following equation

$$\hat{C}_{l,i}(\hat{x},\hat{s}) = A\cosh(\sqrt{\hat{s}}\hat{x}) + B\sinh(\sqrt{\hat{s}}\hat{x}). \tag{19}$$

By differentiation of Eq. 19 in $\hat{x}$, the following equations are obtained from the boundary conditions

$$B\sqrt{\hat{s}} = k_H\frac{\hat{s}+\lambda}{\kappa}A \tag{20}$$

$$A\sqrt{\hat{s}}\sinh(\sqrt{\hat{s}}) + B\sqrt{\hat{s}}\cosh(\sqrt{\hat{s}}) = \hat{N}_i(\hat{s}). \tag{21}$$

Solving for the constants then yields the following expression

$$\hat{C}_{l,i}(\hat{x},\hat{s}) = \hat{N}_i(\hat{s})\frac{k_H\frac{\hat{s}+\lambda}{\kappa}\sinh(\sqrt{\hat{s}}\hat{x}) + \sqrt{\hat{s}}\cosh(\sqrt{\hat{s}}\hat{x})}{k_H\frac{\hat{s}+\lambda}{\kappa}\sqrt{\hat{s}}\cosh(\sqrt{\hat{s}}) + \hat{s}\sinh(\sqrt{\hat{s}})}. \tag{22}$$

As long as mass transport in the UHV environment is assumed to be significantly faster than at ambient conditions, Henry's law at $\hat{x} = 0$ holds and the gas sampling volume is assumed to be ideally mixed, the mass spectrometer signal is directly proportional to $\hat{C}_{l,i}(\hat{x} = 0, \hat{s})$. From Eq. 22 one thus obtains the dimensionless relationship between mass spectrometer signal and partial current density as follows

$$\hat{C}_{l,i}(0,\hat{s}) = \hat{N}_i(\hat{s})H(\hat{s}) \tag{23}$$

$$H(\hat{s}) = \frac{1}{k_H\frac{\hat{s}+\lambda}{\kappa}\cosh(\sqrt{\hat{s}}) + \sqrt{\hat{s}}\sinh(\sqrt{\hat{s}})}. \tag{24}$$

Through back transformation into real space one obtains that the mass spectrometer signal is therefore proportional to the convolution integral of $\hat{n_i}(\hat{t})$ with $h(\hat{t}) = \mathcal{L}^{-1}\{H(\hat{s})\}$

$$\hat{c}_{l,i}(0,\hat{t}) = \int_0^\infty \hat{n_i}(\tau)h(\hat{t}-\tau)\,d\tau. \tag{25}$$

The function $h(\hat{t})$ is termed the impulse response and solely depends on the mass transport parameters for a given analyte. In order to now obtain the partial current density from a measured mass spectrometer signal the inverse problem to Eq. 25 has to be solved, which constitutes the deconvolution of the impulse response from a measured mass spectrometer signal. While deconvolution can be carried out in many different ways, the method used in this article and implemented in the *ixdat* software package consists of calculating the discrete values of the impulse response at a sampling frequency equal to the sampling frequency of the measured mass spectrometer signal by numerical inverse Laplace transformation with the Talbot method and subsequent Wiener deconvolution of this impulse response from the measured mass spectrometer signal as follows

$$\hat{N}_i(f) = \hat{C_{l,i}}(f)\frac{H^*(f)}{H(f)H^*(f) + SNR}. \tag{26}$$

Here, $F(f)$ is the discrete fourier transform of the respective discrete time series, $F^*(f)$ is its complex conjugation and SNR is the signal-to-noise ratio. Finally, $\hat{n_i}(t)$ is obtained by the inverse discrete fourier transform from $\hat{N}_i(f)$. The discrete fourier transform and its inverse are thereby calculated by the Fast Fourier Transform algorithm as implemented in *numpy*.

Sensitivity analysis

In order to asses the influence of the vacuum mass transport on the impulse response, the tubing leading up to the ionization unit is extended by 60 cm (including elbows, which even further slows down molecular flow mass transport in the UHV environment), while keeping the electrochemical cell mounted in order to ensure the same working conditions. Although a slight decrease in the

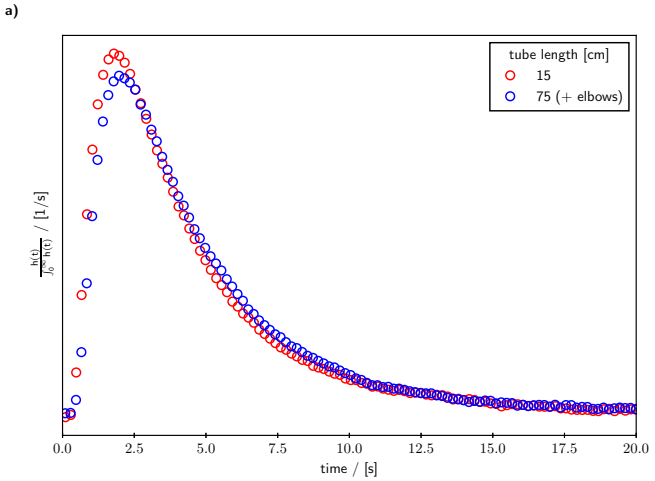

Figure S2: (a) Influence of length of evacuated tubing leading up to the ionization on the impulse response for hydrogen.

impulse response is observed upon increasing the tubing length, the influence is significantly less compared to the influence of working distance and the capillary flow. Consequently, with the configuration that minimizes the mass transport in the UHV environment by minimizing tubing length and maximizing tubing inner diameter, it can be assumed that UHV mass transport is negligible.

The influence of the working distance L was studied by using different thicknesses of Teflon spacers (nominal thickness of 50, 100 and 150 µm). The working distance is then determined by fitting the model to the measured hydrogen impulse response by varying the working distance L. The results for L are around 70 µm larger than the nominal values for all spacer thicknesses, which is probably due to a small indentation of the working electrode into the U-cup assembly. The deviation from the nominal spacer thickness underlines the importance of obtaining the real working distance from a actual measurement to ensure accurate deconvolution. This can either be done by fitting a measured impulse response or by measuring the diffusion limited current of e.g. hydrogen oxidation. This allows to calculate the working distance with the following formula assuming a linear concentration profile under steady state conditions.

$$L = 2F p_{H_2} K_H \frac{D}{J_{lim}} \tag{27}$$

In a separate experiment, the impulse response yielded a distance of 150 µm and the hydrogen oxidation yielded 145 µm.

In order to study the influence of the capillary flow while having the same working distance, the auxiliary gas is the the only free parameter given the fixed geometry of the membrane-chip. Helium, used as a auxiliary gas for the measurements reported in the main text, has a comparably low viscosity leading to a higher capillary flow. On the other hand, argon is more viscous than helium and therefore, if used as a auxiliary gas, leads to a lower capillary flow. Hence, the residence

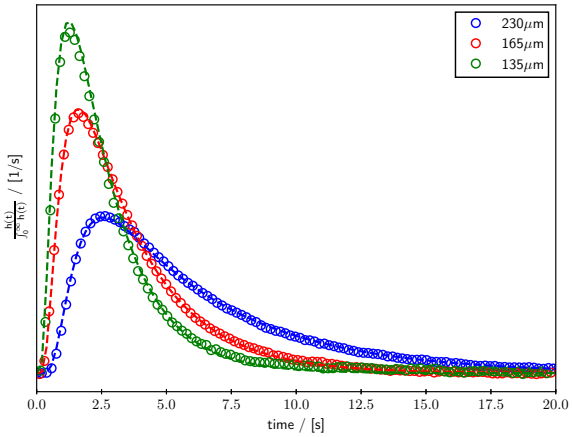

Figure S3: Modeled impulse response (dashed) compared to the measured impulse response (dots) for different working distances, which were obtained by fitting.

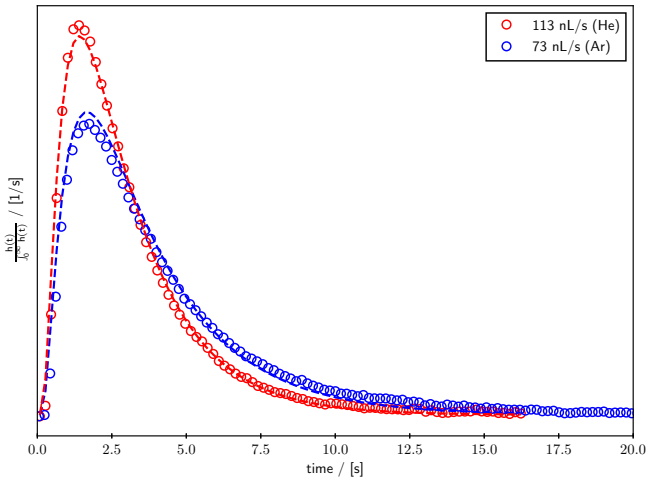

Figure S4: Modeled impulse response (dashed) compared to the measured impulse response (dots) for helium ($113\,\mathrm{nl\,s^{-1}}$) and argon ($73\,\mathrm{nl\,s^{-1}}$) as auxiliary gas.

time in the gas sampling volume can be varied by using argon instead of helium as an inert auxiliary gas. Figure S4 compares the impulse response of hydrogen measured with helium or argon as an auxiliary gas together with the model predictions for the respective capillary flows.

Potential step on oxidized platinum

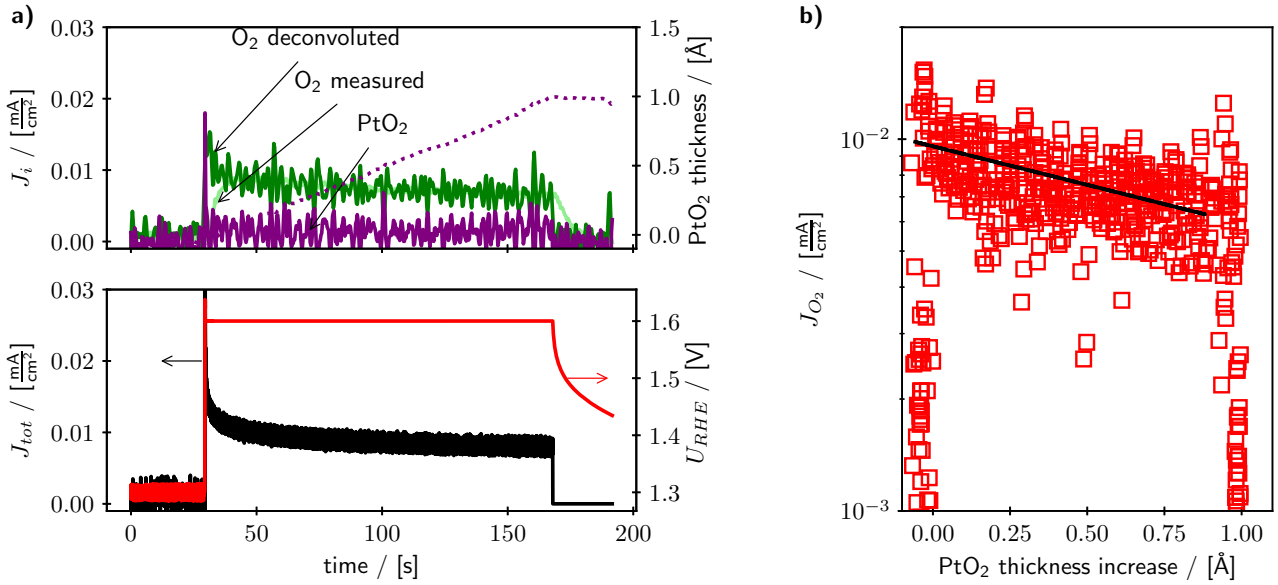

Figure S5: (a) The upper panel shows the deconvoluted partial current density of OER (including the measured MS signal) and PtO_2 formation together with the calculated thickness of the formed oxide during a potential step experiment. Lower panel shows the total current density and voltage as measured by the potentiostat. (b) OER partial current density plotted against the calculted oxide thickness during the potential step experiment displayed in a.

References

(1) Trimarco, D. B. Real-time detection of sub-monolayer desorption phenomena during electrochemical reactions: Instrument development and applications. Ph.D. thesis, Danish Technical University, 2017.